A Finite Element Model of Multi-Layered Laser Sintered Parts

E. M. Weissman[1] and M. B. Hsu[2]

Abstract

A finite element heat transfer analysis is applied to the selective laser sintering of a layered part made from polymer powder. The sintering subroutine in the code is based on the analyses of Scherer [1,2] and Mackenzie and Shuttleworth [3]. The density and conductivity of the particle bed are treated as functions of the void fraction of the bed. The Yagi - Kunii [4] thermal characterization of the powder bed is used to calculate the effective conductivity of the bed. An example is worked for ABS powder.

Introduction

Upon heating, a bed of polymeric powder undergoes a temperature rise and a densification. To better understand this process considerable effort has been expended recently to mathematically model it [5,6]. A successful model would at a minimum provide density (or void fraction) and temperature as a function of time everywhere in the sintering powder bed. Preferably it would also yield the distribution of stresses that can develop in the sintered part as it cools. Inputs for a candidate model include the spatial and time parameters of the input flux, which would include the path followed by the laser beam in scanning out an arbitrary part, the initial temperature of the powder, other thermal boundary conditions and the thermo-mechanical material properties of the constituents of the powder bed and sintered material.

The problem of modeling the sintering of a bed of particles on a microscopic scale (i.e.,smaller than the particles themselves) is a computationally daunting task. If, instead, the particle bed is conceptualized as a continuum with effective thermal properties that may depend on temperature and porosity, the task is made more tractable. This is the approach used in Ref.5 and in this work: conductivity and specific heat of a homogenized particle bed are used in the model. The effective specific heat of the bed is the same as that for the solid particles because of the small mass of air. Thermal conductivity is calculated from the Yagi - Kunii [4] relationship:

$$K_{eff} = \beta(1-\varepsilon)K_s / (1 + \phi K_s / K_g) \qquad \text{(EQ 1)}$$

where $K_{(eff,\ s,\ g)}$ = thermal conductivities: effective, solid, and gas
ε = void fraction
$\beta = 1$
$\phi = 0.034$

While the particle bed is treated homogeneously with respect to its thermal properties, the sintering behavior is idealized in another way: the bed is assumed to consist either of a cubic array of cylinders with open pores, as first suggested by Scherer[1], or, if the density is at least 0.94 of the theoretical maximum, of an array of spheres, as proposed by Mackenzie and Shuttleworth [3]. With these two idealizations we can account for both the heat transfer and resulting softening, flow and coalescence of the irradiated material.

1. BFGoodrich Research and Development, Brecksville, Ohio
2. Marc Analysis Research Corporation, Palo Alto, California

This combined approach to a sintering model (i.e., a 1-D thermal/Scherer model) was first used by Sun et al[5]. In that work they used a finite difference algorithm to follow the sintering process in time and space in a single layer of powder. In this work we have attempted to solve the problem with the finite element method, with our ultimate goal being a full 3-D analysis for a sintered part of arbitrary geometry. Our first steps, which are presented here, demonstrate the successful application of this technique to the same problem solved in Ref. 5, and extend that analysis to the case of a multiply layered part. To carry out the finite element analysis, we have used the MARC finite element package, to which was appended an appropriate user written subroutine to include the sintering submodel. Ultimately we believe that the FEM will provide the necessary flexibility to study the sintering process in parts of complex geometry, which are routinely made by the SLS process. In particular we have used the MARC code because of its ability to solve nonlinear heat conduction equations. Furthermore, MARC is setup to accept user written subroutines.

Thermal submodel

The one dimensional form of the heat transfer equation was used, which is representative of the physical situation of a quickly moving laser heat source scanning over a bed of low thermal diffusivity far from the ends of the scanning path. The equations are therefore:

$$\rho Cp\frac{\partial T}{\partial t} = \frac{\partial}{\partial z}(K\frac{\partial T}{\partial z}) \qquad \text{(EQ 2)}$$

with the following initial and boundary conditions:

$$\begin{aligned} -K\frac{\partial}{\partial z}T(0,t) &= q(t)\ \begin{cases} q_0 \text{ for } 0 \le t \le \tau \\ 0 \text{ for } t > \tau \end{cases} \\ T(z,t) &\to 0 \quad \text{for } z \to \infty,\ t > 0 \\ T(z,0) &= T_0 \end{aligned} \qquad \text{(EQ 3)}$$

where: T = T(z,t) = temperature field with respect to position and time
K = effective bed conductivity
C_p = specific heat
ρ = density
q = laser flux
τ = laser pulse duration

The boundary condition at z = 0 assumes that all the energy incident on the bed is absorbed. At a given temperature the thermal properties in EQ 2 will change with time due to the sintering process, which causes a reduction in void fraction. In this work only the density and conductivity changes are tracked and updated. An average value for the specific heat is used. The properties may also be explicit functions of temperature, but we have ignored this dependency in this work. Future extensions of the model will include it.

The functional dependency of the conductivity on void fraction is given in EQ 1; that of the density ρ is given by:

$$\rho = \rho_s(1-\varepsilon) \qquad \text{(EQ 4)}$$

where ρ_s = full density.

The finite element approximation to the heat conduction equation EQ 2, using effective thermal conductivity EQ 1 and modified density EQ 4, is discussed in a later section.

The Scherer and Mackenzie-Shuttleworth Models

To follow the evolution of the change in density or void fraction as a function of time and temperature, the Scherer model was used for the low density phase of the process ($\rho \leq 0.94\ \rho_s$), and the Mackenzie - Shuttleworth model was used for higher densities. Both of these models assume that the surface energy reduction of the sintering powder drives the process through viscous mass flow dissipation. At the lower densities the powder is assumed to consist of an open pore network of cylinders arranged cubically, with the cylinder diameters equal to the particle diameter and the cylinder lengths proportional to the pore diameter. As sintering proceeds, the cylinder heights collapse, reducing the void fraction in the powder bed, until the cylinder walls touch one another. At this point the situation can be described by contiguous spheres with closed pores. The essential relationships for our needs that follow from this approach are:

$$\frac{\partial e}{\partial t} = -\frac{M}{\eta}\frac{(3\pi)^{1/3}}{6}\frac{2-3cx}{\sqrt[3]{x(1-cx)^2}} \qquad \text{(EQ 5)}$$

for open pore, low density powder beds and partially sintered parts(i.e. $\rho \leq 0.94\rho_s$), and

$$\frac{\partial e}{\partial t} = -\frac{M}{\eta}\frac{1}{2}\left(\frac{4\pi}{3}\right)^{1/3}\left(\frac{\rho_s}{\rho}-1\right)^{2/3} \qquad \text{(EQ 6)}$$

for closed pore (i.e. $\rho > 0.94\rho_s$) beds and parts. These equations describe the contraction or free strain rate $\frac{\partial e}{\partial t}$ of the sintering material. The quantity M appearing in both equations is given by:

$$M = \gamma n^{1/3}, \qquad \text{(EQ 7)}$$

where γ = surface energy and n = the number of particles per unit volume of fully densified material. The quantity η is the viscosity of the material, which is a function of temperature, given by [5]:

$$\eta = A\exp\left(\frac{\Delta E}{RT}\right), \qquad \text{(EQ 8)}$$

with A and ΔE constants. In the work reported here M and η were determined separately from EQs 7 and 8, respectively.This requires the separate determinations be made of surface energy,γ, activation energy, ΔE, and the constant A. In principle, however, the ratio M/η can be obtained directly from density vs. time measurements, as was pointed out by Scherer[1].

The strain rate for low density sintering, EQ 5, is also seen to be a function of x. This is the aspect ratio of the cylinders that make up the unit cell in that model. (The constant c in that equation is $8\sqrt{2}/3\pi$.) In the Mackenzie - Shuttleworth model, EQ 6, strain rate is a function of the ratio of the densities of the fully sintered material ρ_s and the actual density of the bed ρ.

As the particles sinter, the void fraction ε drops. The Scherer model gives an expression for ε as a function of the cylinder aspect ratio in the unit cell as:

$$\varepsilon = 1 - 3\pi x^2 + 8\sqrt{2}x^3 = 1 - \frac{\rho}{\rho_s} \qquad \text{(EQ 9)}$$

Given a value of the particle bed density or void fraction, EQ 9 can be used to find the corresponding value of x which in turn can be substituted into EQ 5 to find a new strain increment Δe and a new $e_{i+1} = e_i + \Delta e$.

When the subroutine is called, the viscosity $\eta(T)$ is found by EQ 8. If the density is greater than 0.94 of full density, the Mackenzie - Shuttleworth model holds and EQ 6 is used to find the updated free strain. If the density is less than this value, EQ 9 is used to find the aspect ratio x of the cylinders in the Scherer model, and then EQ 5 calculates the updated free strain.To find the updated void fraction ε and density ρ corresponding to the strain e, another relationship must be used:

$$\varepsilon = 1 - \frac{\rho_0}{\rho_s} exp(-3e) \quad . \qquad \text{(EQ 10)}$$

This equation applies to any material undergoing isotropic true strain, i.e., $e = \ln(l/l_0)$, where l and l_0 are the final and initial lengths of any line undergoing a strain e. The result from EQ 10 is fed back to EQ 1 to find the updated conductivity, and the subroutine is exited

Finite Element Model

This section describes the implementation of the previously discussed sintering model into a general purpose finite element program and then presents some finite element results validating these numerical models. A discussion on the technical approach is given first and then results of single and multi-layer sintering processes are presented.

Technical Approach

In the finite element formulation the discretization of both the space and the time variables serves as the basis of the approximation. The region of interest s in the sintering material is subdivided into elements, and the temperature T(s) within an element is interpolated from the nodal values T of the element through the interpolation functions N(s),

$$T(s) = N(s)\,T \qquad \text{(EQ 11)}$$

The governing equation of the heat conduction problem can be obtained from the minimization of weighted residuals of the differential equation, resulting in the matrix equation :

$$C(T)\,\dot{T} + K(T)\,T = Q \qquad \text{(EQ 12)}$$

where C(T) and K(T) are the temperature dependent heat capacity and thermal conductivity matrices, T is the nodal temperature vector, $\dot{T}$ is the time derivative of the temperature vector, and Q is the heat flux vector.

The system matrices C(T) and K(T) are obtained from the summation of all element matrices $C_e(T)$ and $K_e(T)$ in the mesh as

$$\begin{aligned} C(T) &= \sum C_e(T) \\ K(T) &= \sum K_e(T) \end{aligned} \qquad \text{(EQ 13)}$$

The element matrices $C_e(T)$ and $K_e(T)$ can be evaluated from the following volume integrals over the volume of the element:

$$\begin{aligned} C_e &= \int_V N^T \rho c N dV \\ K_e &= \int_V B^T k B dV \end{aligned} \qquad \text{(EQ 14)}$$

In EQ 14 ρ is the mass density, c is the specific heat and k is the thermal conductivity of the material. The matrices N and B are the shape function and temperature gradient, respectively. As discussed in the previous section, the sintering material can be characterized by effective conductivity k_{eff} and density ρ, which are dependent on the void fraction ε. It is obvious that once k_{eff} and ρ are given then both the heat capacity and the conductivity matrices in the finite element equation can be easily calculated:

$$C_e = \int_V N^T \rho(\varepsilon)\, cN dV$$
$$K_e = \int_V B^T k_{eff}(\varepsilon)\, B dV \qquad \text{(EQ 15)}$$

Note that c and k_{eff} in the above equation can also be dependent on temperature.

Although the time variable can be discretized the same way as space variables, a finite difference scheme is usually chosen in the finite element analysis. The selection of a backward difference scheme yields the following expression:

$$\left[\frac{1}{\Delta t} C(T) + K(T)\right] T_n = Q_n + \frac{1}{\Delta t} C(T)\, T_{n-1} \qquad \text{(EQ 16)}$$

Equation 16 computes nodal temperatures for each time increment Δt. It can be seen that starting from the initial conditions the temperature is calculated at an initial time step for all elements. The effective conductivity, density (void fraction) and free strain are updated in the sintering subroutine. The new conductivities and densities are then used to find the temperatures at the next time increment.

Case Studies

During this investigation two finite element heat conduction analyses were carried out for validating the previously discussed sintering and heat transfer models. The two analyses simulate a single and a multi-layered sintering processes, respectively. Both the 2-node three-dimensional heat element and the 4-node two-dimensional planar heat element were used for the analyses and identical results were observed. The numerical results presented in this section are those of the 4-node model.

As shown in Fig. 1 the single-layered model consists of 30 4-node elements and 62 nodes. A concentrated laser flux q_0 was applied at one end (nodes 31, 62) of the model for a duration of τ seconds. Both the initial and boundary conditions and the material properties were obtained from Ref. 7 (Table 1). Figures 2 and 3 show time variations of applied laser flux and temperature at the point of application (node 31). The void fraction distribution along the depth of the model at 0.008 seconds is depicted in Fig. 4. The characteristics of the sintering process can be clearly seen from these results.

The multi-layered model is similar to the single-layered model but has 90 elements for three layers. The same concentrated laser flux was applied sequentially in three passes to the end of the submodel for each layer (nodes 31 and 122 for the first layer, nodes 61 and 152 for the second layer and nodes 91 and 182 for the third layer). The duration of each flux application was the same τ seconds. Both the initial/boundary conditions and material properties were the same as in the single-layered model.

In order to deal with the multi-layered situation the program options ACTIVATE and DEACTIVATE were used for the representation of the first pass (elements 1 to 30), the second pass (elements 1 to 60) and the third pass (elements 1 to 90) of the sintering process. Although the total number of elements in the model is 90, with the ACTIVATE and DEACTIVATE options there are actually 30 active elements in the first pass, 60 elements in the second pass and 90 elements in the third pass analyses, respectively.

Figure 5 shows a finite element model using the 4-node planar heat transfer element for the layered model. Variations in time of laser flux and temperature are depicted in Figs. 6 and 7, respectively. Note that a transient time of 0.02 seconds is assumed for each pass. Figures 8,9,10 and 11,12, and 13 show distributions along the layer depth of temperature and void fraction at transient times of 0.02, 0.04 and 0.06 seconds, respectively.

The finite element results presented in this section are reasonable. However, a parametric study would be very useful in determining the important parameters in the process. The intensity and duration of laser flux, temperature dependency of material properties, as well as thermal and mechanical boundary conditions are of great importance in the process.

TABLE 1. Initial conditions, boundary conditions and material properties (ABS) [Ref. 7]

Boundary Conditions:

Laser flux, q_0	6.6×10^7 W/m^2
Laser duration, τ	4.76×10^{-4} s

Initial Conditions:

Initial bed temperature, T_0	293 °K
Initial density, ρ_0	526 Kg/m^3

Material constants:

Full Density, ρ_s	1095 Kg/m^3
Viscosity coefficient, A	5.41×10^{-18} Pa·s
Activation energy, ΔE	20638 °K
Surface energy, γ	45×10^{-5} J/m^2
Particle bed specific heat, C_p	1580 J/°K·Kg
Conductivity of solid ABS, K_s	0.21 W/°K·m
Conductivity of air, K_g	0.026 W/°K·m

Conclusion

We have presented the first results of efforts to apply the finite element method to the problem of laser sintering. This has been accomplished by incorporating a subroutine for the sintering models of Scherer and Mackenzie - Shuttleworth into the Marc heat conduction equation solver. Using this approach we have been able to predict not only the behavior in a single layer of material, but also how a bed of powder sinters that is laid down in discrete layers in time. Our next efforts will focus on extending the model to two dimensions in order to assess edge effects.

References

1. Scherer, G., "Sintering of Low-Density Glasses: I, Theory," J. Am. Ceramic Soc., **60**, [5 - 6], pp 236 - 239, 1977.
2. Scherer, G., "Viscous Sintering under a Uniaxial Load," J. Am. Ceramic Soc., **69**, [9], pp 206 - 207, 1986.
3. Mackenzie, J., and Shuttleworth, R., "Phenomenological Theory of Sintering," Proc. Phys. Soc. London, **62**, [12-B], pp 833- 852, 1949.
4. Yagi, S., and Kunii, D., "Studies on Effective Thermal Conductivities in Packed Beds," A.I.Ch.E. Journal, **3**, 3, pp 373 - 381, 1957
5. Sun, M., Beaman, J., and Barlow, J., "Parametric Analysis of the Selective Laser Sintering Process," Proc. Solid Freeform Fabrication Sym., pp 146 - 154, August 1990.
6. Nelson, C., and Barlow, J., "Sintering Rates in the Selective Laser Sintering Process," Proc. Solid Freeform Fabrication Sym., pp 164 - 170, August 1990.
7. Sun, M., Private communication

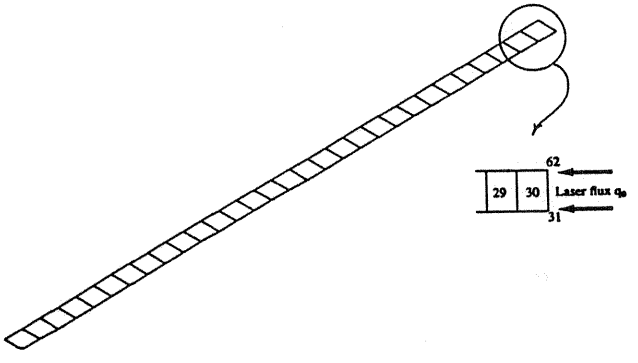

Fig. 1. Finite Element Mesh
(single-layered model 30 elements)

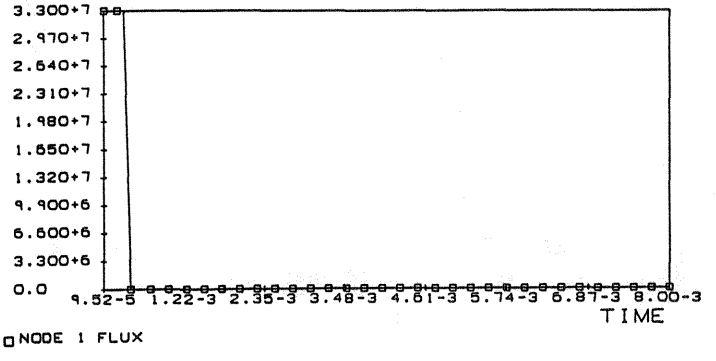

Fig. 2. Laser Flux vs Time
(single-layered model)

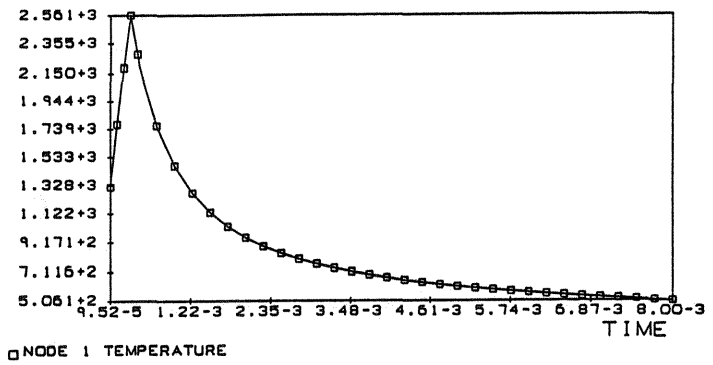

Fig. 3. Node 1 Temperature vs Time (single-layered model)

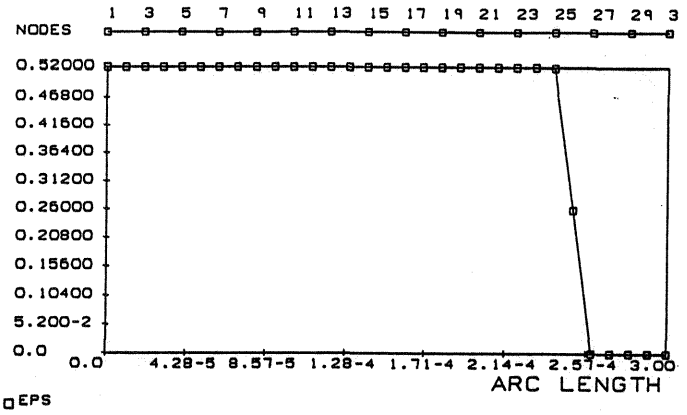

Fig. 4. Void Fraction vs Layer Depth (single-layered model) time = 0.008 sec.

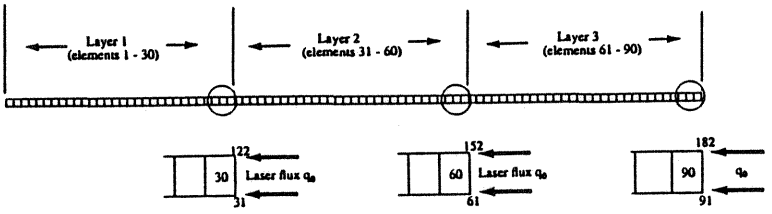

Fig. 5. Finite Element Mesh (multi-layered model 90 elements)

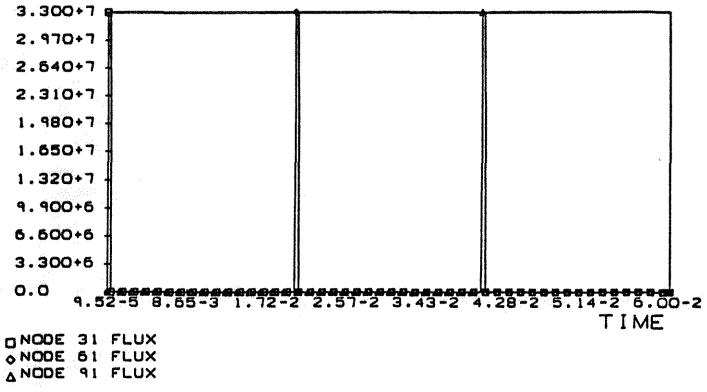

Fig. 6. Laser Flux vs Time (multi-layered model)

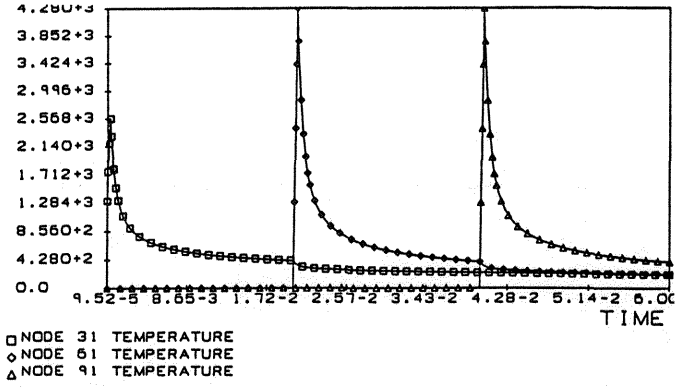

Fig. 7. Nodal Temperatures vs Time (multi-layered model)

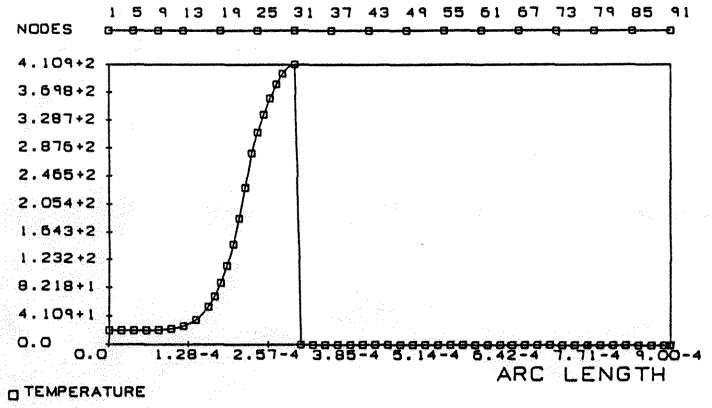

Fig. 8. Temperature vs Layer Depth (multi-layered model) time = 0.02 sec.

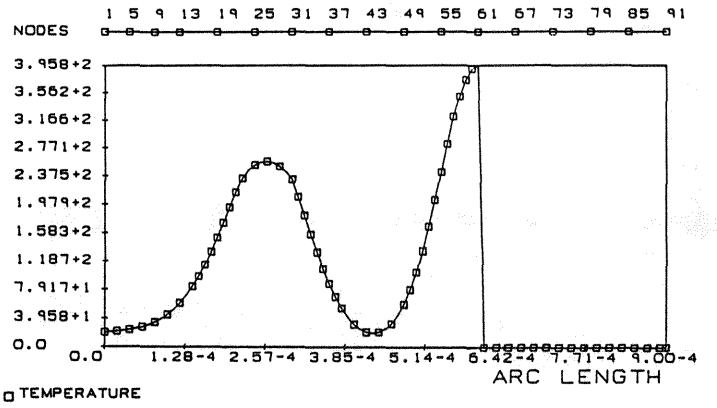

Fig. 9. Temperature vs Layer Depth (multi-layered model) time - 0.04 sec.

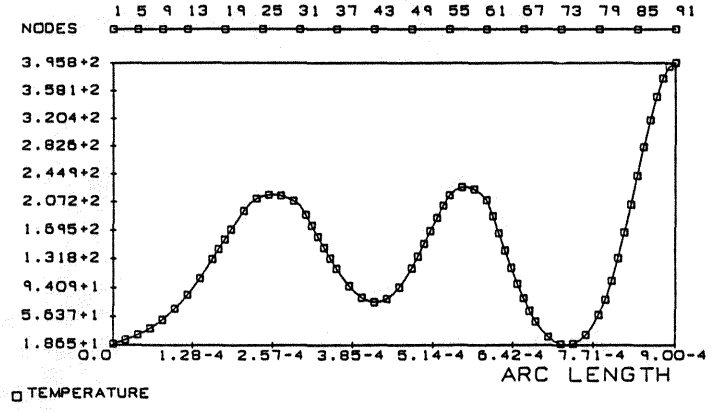

Fig. 10. Temperature vs Layer Depth (multi-layered model) time = 0.06 sec

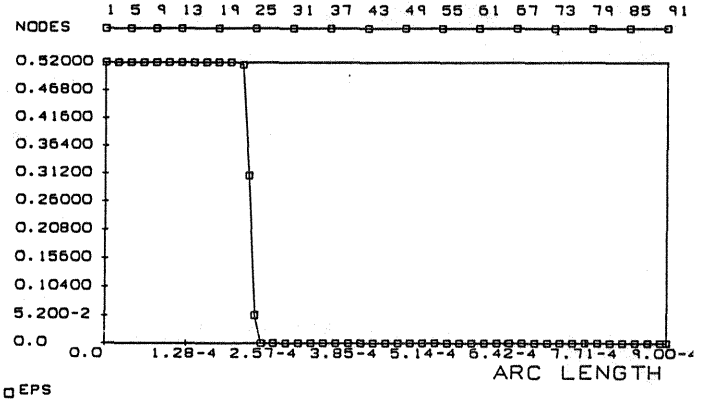

Fig. 11. Void Fraction vs Layer Depth (multi-layered model) time = 0.02 sec.

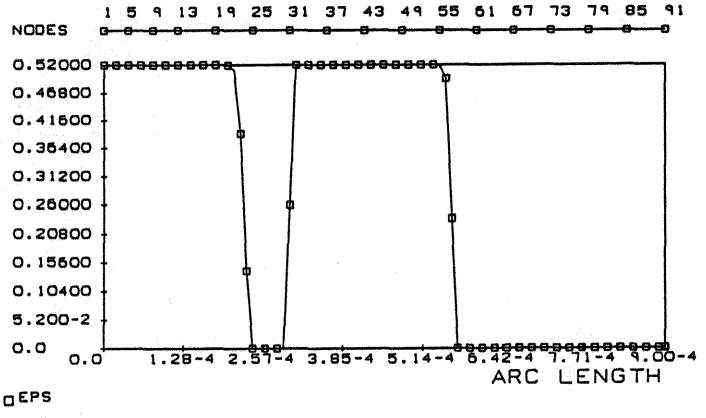

Fig. 12. Void Fraction vs Layer Depth (multi-layered model) time = 0.04 sec.

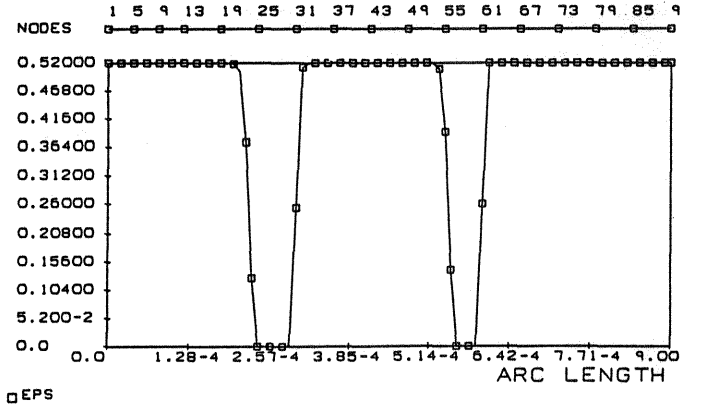

Fig. 13. Void Fraction vs Layer Depth (multi-layered model) time = 0.06 sec.